Impact of Pressure Wire on Fractional Flow Reserve and Hemodynamics of the Coronary Arteries: A Computational and Clinical Study

Zhengzheng Yan, Zhifeng Yao, Weifeng Guo, Dandan Shang, Rongliang Chen, Jia Liu, Xiao-Chuan Cai, and Junbo Ge

***Abstract*— Objective: Noninvasive fractional flow reserve (FFR) has been extensively studied and gained clinical recognition. However, the effect of an interventional catheter and a pressure wire in the arteries on the noninvasive FFR was not considered in previous studies. We provide quantitative analysis of how a catheter and a pressure wire can affect the estimation of noninvasive FFR using computational fluid dynamics (CFD) techniques. Methods: Six patients are studied. We calibrate our CFD model with patient-specific conditions so that the noninvasive FFR matches the FFR measured by the pressure wire. Then, we numerically remove the pressure wire and compute the noninvasive FFR again. This allows us to analyze the effect of the pressure wire on FFR. Results: The presence of a catheter and a pressure wire can reduce distal pressure from -0.1 mmHg to -8.1 mmHg, resulting in a reduction of FFR by 5.8% in average (0.012 to 0.107 or -1.2% to -16.8%). The insertion also reduces the time-averaged flow rate at the stenosis by up to 16.2% (4.9% in average). Conclusion: The impact of the pressure wire on the measured FFR depends on the characteristics of the patient-specific lesion. Significant linear correlations are found between the minimum diameter of the stenotic arteries and the reduction in FFR. Significance: The impact we found may contribute to provide a correction and improve the estimation of the noninvasive FFR technique for use in clinical practice.**

***Index Terms*— Cardiovascular physiology, computational fluid dynamics, coronary artery disease, fractional flow reserve, pressure wire**

I. Introduction

CORONARY artery disease is one of the most common cardiovascular diseases and the leading cause of death and disability [1]. Coronary artery disease occurs when the coronary arteries that supply blood to the myocardium become narrowed. However, studies have shown that the anatomical significance, such as coronary angiography, has a weak correlation with the functional importance of epicardial coronary artery disease [2]. When blood flow is insufficient to meet the myocardium's demand, myocardial ischemia happens and in turn causes symptoms and affects patient outcome. Therefore, the functional significance represented by ischemia assessment is more valuable than anatomical significance in terms of symptom diagnosis and revascularization [3]. In order to quantify the degree of myocardial ischemia, fractional flow reserve (FFR) has become an important clinical indicator to determine how much the stenosis impedes the blood delivery to the myocardium. FFR is defined as the ratio between the maximum achievable blood flow in a stenotic coronary artery and the theoretical maximum flow in the same coronary artery if it was normal. In clinical practice, a catheter is inserted at the entrance of the coronary artery, and the pressure sensor on it returns the time-averaged proximal pressure P_a, and at the same time, the pressure sensor on the tip of the pressure wire passing through the stenosis returns the time-averaged distal pressure P_d, FFR is then calculated as the ratio P_d/P_a under the condition of maximum myocardial hyperemia. FFR equals to 0.8 is the threshold at which revascularisation should be considered [4], [5]. This FFR measurement is the current gold standard test to assess the haemodynamic significance of coronary lesions [6], [7].

It is worth pointing out that the presence of the pressure wire in the coronary artery changes the patient's hemodynamic characteristics, especially in the vessel with stenosis, because the diameters of the catheter and the pressure wire are sometimes comparable to the diameter of the coronary artery. Previous studies [8], [9] have shown that, the insertion of pressure wire aggravates the obstructive effect of the lesion and therefore reduces the coronary flow and increases the pressure drop. Tadaoka et al. [10] presented an experimental method to study the influence of the catheter on the flow velocity in a straight tube under various flow rates. Torii et al. [11] simulated the effect of catheters of different diameters inserted in a 180° curved tube 3 mm in diameter. For an inlet flow velocity

This work was supported in part by the NSFC under Grant 11901559 and 62161160312, Shenzhen RCYX20200714114735074 and JCYJ20220531100611025, and Shanghai 22ZR1426000. (Corresponding author: Rongliang Chen and Xiao-Chuan Cai. Zhengzheng Yan and Zhifeng Yao contributed equally to this work.)

Zhengzheng Yan, Rongliang Chen (e-mail: rl.chen@siat.ac.cn) and Jia Liu are with Shenzhen Institutes of Advanced Technology, Chinese Academy of Sciences, Shenzhen, China.

Zhifeng Yao and Junbo Ge are with the Department of Cardiology, Zhongshan Hospital, Fudan University, Shanghai, China, and Shanghai Municipal Institute of Cardiovascular Diseases, Shanghai, China.

Weifeng Guo is with the Department of Radiology, Zhongshan Hospital, Fudan University, Shanghai, China.

Dandan Shang is with the Department of Cardiology, Shenzhen Second People's Hospital, Shenzhen, China.

Xiao-Chuan Cai is with the Department of Mathematics, University of Macau, Macau, China (e-mail: xccai@um.edu.mo).

of $0.1\,\mathrm{m/s}$, the presence of a catheter increases pressure drop between the inlet and probe tip by 1.3–4.3 mmHg depending on its diameter ranging from 0.3 mm to 1.0 mm. At 5.0 mm downstream from the probe tip, the blockage caused by the catheter will reduce the velocity by about 15–21%. Rajabi et al. [12] used an analytical approach to study the effect of the pressure wire on its contribution of loss due to momentum change and viscous loss to the translesional pressure drop. Based on a axisymmetric geometry of stenosis, this research observed that pressure wire insertion has greater contribution to the rise in viscous loss (increase by 2.14 and 2.72 times for 64% and 90% area stenosis, respectively) than loss due to momentum change (1.34% increase for 64% area stenosis and 25% decrease for 90% area stenosis). Roy et al. [13] compared the vasodilation-distal perfusion pressure curve and hemodynamic analyses for pathophysiological flow and constructed the linear correlation ($\mathrm{FFR_m}$=$\mathrm{FFR_m^g}\times$0.79+0.21 for 0.35 mm pressure wire) between FFR without ($\mathrm{FFR_m}$) and with ($\mathrm{FFR_m^g}$) the pressure wire.

All previous studies have assumed either the flow is two-dimensional or the flow is three-dimensional but the geometry of the artery is idealized. As a results, the studies do not reflect the true interference of the pressure wire and the hemodynamics of the patients. Moreover, in clinical practice, it is usually necessary to choose a pressure wire with different size (diameter) according to the actual physiological condition of the patient. A fixed diagnostic standard indicator (FFR=0.8) for the clinical diagnosis even if pressure wires of different sizes used. This obviously ignores the influence of the catheter and pressure wire, and the loss of accuracy is not counted for. On the other hand, some noninvasive FFR technologies have been approved by regulatory authorities for clinical diagnosis in recent years. $\mathrm{FFR_{CT}}$ [14], [15] as an example, the geometry of the artery is reconstructed from the coronary computed tomography angiography (CCTA) images excluding the catheter and the pressure wire model and the numerically computed FFR values are compared with the invasive FFR values (obtained with the catheter and the pressure wire). The same cut-off value (i.e., 0.8) is used to determine the negative and positive cases. Researchers of [16], [17] have reported that noninvasive FFR techniques can provide acceptable diagnostic accuracy for clinicians. However, in the subgroups with intermediate stenoses and FFR values between 0.70 and 0.85, the discriminatory performance of noninvasive FFR techniques is weaker than the other subgroups [18], [19], therefore it requires more accurate discrimination for these subgroups. To improve the diagnostic accuracy of the noninvasive FFR, the impact of the pressure wire on FFR needs to be studied more carefully. In this paper, we investigate numerically how the catheter and pressure wire effect the pressure drop, and whether the FFR simulated by the noninvasive method requires a correction.

The objective of the paper is to study the impact of the pressure wire on the FFR values of actual patients using a CFD algorithm. The computations are carried out in pairs with identical patient information and one with a pressure wire and one without. Results for six patients are analyzed in detail. In addition, we also analyze the influence of the diameter of the stenosis or the stenosis ratio on the FFR values, and the flow fields with the presence of the pressure wire.

II. Materials and Methods

Six patients from Zhongshan Hospital (Shanghai, China) with various degree of stenosis are used in the study and their characteristics are listed in Table I. Since the collected patient-specific data are anonymized and our study is observational and retrospective in nature, patient approval and informed consent are waived. After the CCTA acceptance, all subjects received the invasive coronary angiography scan, during which FFR was measured. A 6F (2.0 mm) guiding catheter (EBU3.5, Launcher, Medtronic, Minneapolis, MI, USA) was first placed at the entrance of the coronary artery, and then a 0.014 inch (0.36 mm) pressure wire (Runthrough NS Hypercoat; Terumo Corp. Tokyo, Japan) was advanced to the distal end of the left anterior descending coronary artery or the left circumflex coronary artery.

TABLE I
Patient Characteristics.

Patient ID	Gender	Age (year)	SBP (mmHg)	DBP (mmHg)	Heart Rate (bpm)	SR	SP
1	Male	49	120	70	70	65.8%	LAD
2	Female	69	106	68	70	50.6%	LAD
3	Male	76	130	70	80	17.0%	LAD
4	Male	71	118	76	72	55.0%	LCX
5	Male	77	110	70	68	52.0%	LAD
6	Male	62	110	60	70	64.7%	LCX

Notes: SBP = systolic blood pressure; DBP = diastolic blood pressure; bpm = beats per minute; SR = stenosis ratio; SP = location of the lesion; LAD = left anterior descending coronary artery; LCX = left circumflex coronary artery. SBP and DBP are measured in the brachial artery during coronary computed tomography angiography scan. SR are estimated from coronary angiography images.

A. Vascular reconstruction and numerical grid generation

Two images are taken for each patient; one CCTA image without the catheter and the pressure wire, and one digital subtraction angiography (DSA) image with the catheter and the pressure wire. FFR is measured at the same time when the DSA is taken. These two types of images are commonly used technique in the diagnosis of coronary artery disease, and can provide two-dimensional layered and dynamic images of three-dimensional coronary artery under X-rays, respectively. CCTA images and DSA images are used to reconstruct the geometry of the artery, the catheter and the pressure wire. Specifically, we obtain the 3D geometry of the coronary artery from the multi-slice CCTA image, which parameters are set as: the slice thickness is 0.75 mm, the pixel size is 0.430 mm, the image resolution is 512×512 and the total number of slices is 375. Typically, the images acquired during diastole (e.g., at 75% of R-R interval) are applied for the reconstruction. Then, the reconstructed geometry is further confirmed and corrected by the DSA images, especially for the subsegment of the artery with stenosis lesion, to ensure that the reconstructed artery conforms to the physiological anatomical model. Fig. 1 shows the reconstructed coronary artery as well as its centerline based

on the CCTA images. This geometrical model of the artery will be meshed and used to simulate the hemodynamics without the pressure wire and the catheter.

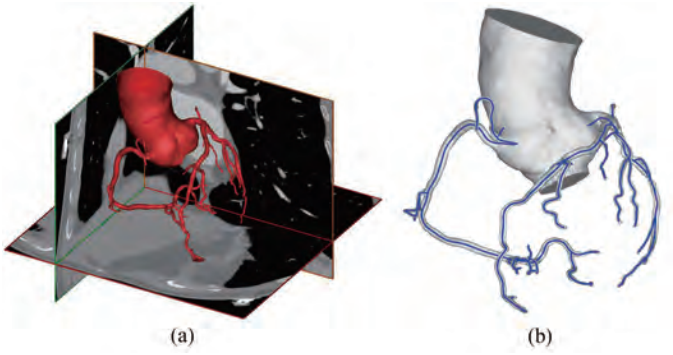

Fig. 1. Geometry of the reconstructed coronary artery and its centerline. (a) Based on coronary computed tomography angiography images, we first reconstruct the three-dimensional geometry of coronary artery. (b) Then, under the assumption that the pressure wire is placed along the centerline of the blood vessel, we generate the centerline (blue) of the geometry for positioning pressure wire.

In addition to the geometry of the artery, we also need to place the pressure wire and the catheter in the artery during interventional surgery. There are several sizes for the catheter and the pressure wire (e.g., 4F, 5F and 6F for the catheter), the doctor chooses the size of the pressure wire and the catheter according to the patient's physical condition. In this paper, 6F (2.0 mm in diameter) catheter and 14" (0.36 mm in diameter) pressure wire are used for all six patients.

During the operation, the catheter and the pressure wire are moved by the doctor, and their locations are determined by the surgeon. Ideally, the pressure wire should be aligned with the vascular centerline, and away from the vascular wall to reduce the error of the pressure sensor. In this study, we assume that the catheter and the pressure wire are solid cylinders and the pressure wire is placed along the centerline of the blood vessel. It should be noted that the pressure wire may not be in the ideal position due to the pulsating effect of the blood flow. The DSA images provide a good reference, as Fig. 2 shown, for the actual position of the pressure wire. The position of the catheter can also be located from DSA images following the clinical guidelines [20]. Fig. 2 also shows the reconstructed geometry of the coronary artery, the catheter and the pressure wire. This geometrical model will be meshed and used to simulate the hemodynamics with the impact of the catheter and the pressure wire, and the measured FFR.

Unstructured tetrahedral meshes are used for the spatial discretization of the computational domains, and finer meshes are generated near the vascular wall and the surfaces of the catheter and the pressure wire. In order to accurately capture the hemodynamic details around the pressure wire, the maximum size of tetrahedral elements on the surfaces of the pressure wire is set to 0.01 mm. For the patients under consideration, the number of elements is over five million in order to capture the details of the blood flow due to the presence of catheter and pressure wire. The computational meshes of the coronary with and without the catheter and the pressure wire are shown in Fig. 3.

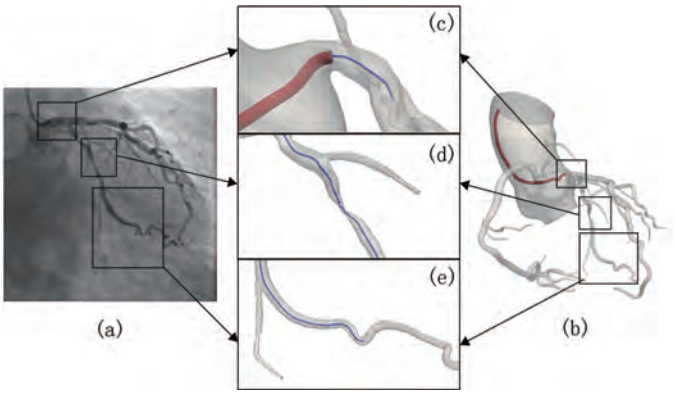

Fig. 2. Reconstruction of the catheter and the pressure wire. (a) The digital subtraction angiography images provide a good reference for the actual positions of the catheter and the pressure wire. (b) The geometry of the catheter (red) and the pressure wire (blue) are merged with the geometry of vessel. Local view in: (c) The junction of the catheter and the pressure wire, also the entrance to the coronary artery. (d) Near the lesion. (e) Near the tip of the pressure wire and measurement point.

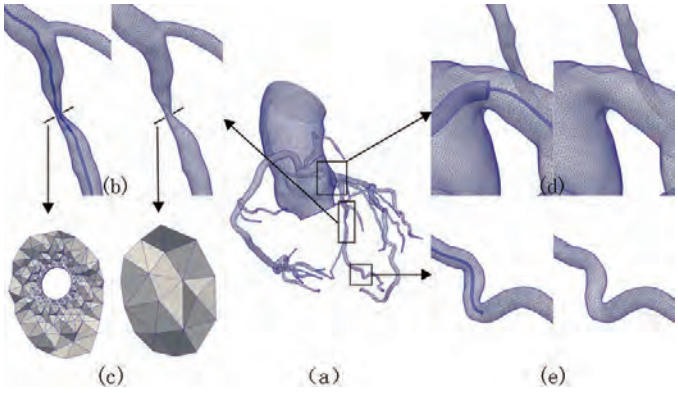

Fig. 3. Comparison of the computational mesh of the coronary tree. (a) Global view of mesh with the catheter and the pressure wire. (b) Near the stenosis. (c) At the cross-section of the stenosis. (d) At the intersection of the pressure wire and the catheter near the entrance of the coronary artery. (e) Near the end of the pressure wire.

B. Flow Model and physiological boundary conditions

We assume the blood flow in the coronary artery is transient, incompressible and laminar. Moreover the blood flow is treated as a Newtonian fluid with the kinematic viscosity $\mu = 0.035\,\mathrm{cm}^2/\mathrm{s}$ and density $\rho = 1.050\,\mathrm{g}/\mathrm{cm}^3$. The Navier-Stokes equations are used to describe the unsteady blood flow on a bounded computational domain Ω.

$$\rho\left(\frac{\partial \mathbf{u}}{\partial t} + \mathbf{u}\cdot\nabla\mathbf{u}\right) - \nabla\cdot\sigma = \mathbf{f}, \tag{1}$$

$$\nabla\cdot\mathbf{u} = 0 \quad \text{in} \quad \Omega, \tag{2}$$

where $\mathbf{u}$ is the fluid velocity, ρ is the constant blood density, μ is the blood viscosity and $\mathbf{f}$ denotes the external force. $\sigma = -p\mathbf{I} + \mu(\nabla\mathbf{u} + (\nabla\mathbf{u})^{\mathsf{T}})$ is the Cauchy stress tensor, p denotes the fluid pressure, and $\mathbf{I}$ is the unit tensor.

A time-varying volume flow rate Q_{in} related to the patient's cardiac output is used as the inflow boundary condition. Considering the total coronary blood flow Q_c is approximately 4.5% of the cardiac output and proportional to myocardial mass by allometric scaling laws, in this work, Q_{in} is derived

from the patient-specific myocardial volume V_m. The profile of Q_{in} is determined using a variant of the aortic flow waveform introduced in [21], as shown in Fig. 4.

$$Q_{in} = Q(V_m, t) \quad \text{on} \quad \Gamma_I. \tag{3}$$

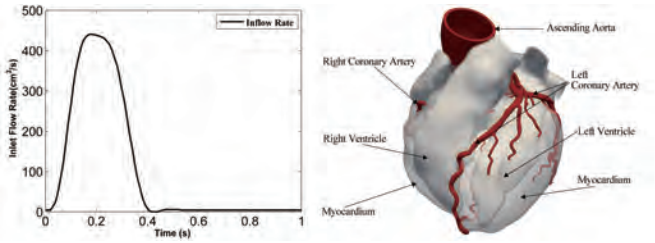

Fig. 4. Time-varying inflow rate profile and reconstructed myocardium. The volume of patient-specific myocardium $\boldsymbol{V_m}$ was measured by the segmented geometry, and used to construct the time-varying inflow boundary condition.

A no-slip condition is imposed on the vascular walls, and also on the surfaces of the catheter and pressure wire; i.e.,

$$\mathbf{u} = \mathbf{0} \quad \text{on} \quad \Gamma_W. \tag{4}$$

A transient RCR model introduced in [22] is imposed on the outlet boundary Γ_O. On the k-th artery outlet, the model has a proximal resistance R^k in series with a parallel arrangement of a capacitance C^k and a distal resistance R_d^k. Specifically, at time t, the time-varying blood pressure $p(t)$ on the k-th artery outlet is computed through the following formula,

$$\begin{aligned} p^k(t) = [p^k(0) - R^k Q^k(0) - p_d^k(0)]e^{\frac{-t}{\tau^k}} + p_d^k(t) \\ + R^k Q^k + \int_0^t (\frac{e^{-(t-\bar{t})/\tau}}{C^k}) Q^k(\bar{t}) d\bar{t}, \end{aligned} \tag{5}$$

where $p^k(0)$ is the initial pressure assumed to be the patient-specific diastolic blood pressure and $p_d^k(t)$ is the downstream pressure assumed to be zero. Q^k is the volume flow rate through the k-th outlet calculated by,

$$Q^k = \int_{\Gamma^k} \mathbf{u}(t) \cdot \mathbf{n} \, d\mathbf{\Gamma}, \tag{6}$$

where $\mathbf{n}$ is the outward unit surface normal to the k-th outlet Γ^k. $\tau^k = R_d^k C^k$ and R_d^k is obtained by the relation

$$R_d^k = \frac{P_b}{Q^k}, \tag{7}$$

where P_b is the mean brachial pressure from the measured systolic and diastolic blood pressure. The resistance and capacitance of the k-th coronary artery branch outlet are distributed by Murray's power law.

C. Simulation solver

The presence of the pressure wire and catheter will considerably increase the complexity of the CFD calculation. Firstly, the exact location of the pressure wire and the catheter are not easy to identify since the pressure wire may move with the flow. Secondly, the presence of the pressure wire often causes a multi-scale problem in the sense that in certain part of the artery the diameter of the wire is neglectably smaller than the diameter of the artery, but in other part of the artery (with stenosis) the diameter of the wire and the artery are comparable to each other. The required high resolution will greatly increase the computational cost, at the same time such transient flow also needs a very small time step.

In this work, a fully implicit second-order backward differentiation scheme is applied for the temproal discretization of the governing equations and a stabilized P_1-P_1 finite element method for the spatial discretization of the model on a fully unstructured tetrahedral mesh. The resulting sequence of large, sparse, highly nonlinear systems of algebraic equations are solved by the parallel Newton-Krylov-Schwarz algorithm [23]–[25], that consists of a sequence of Newton iterations embedded with Krylov subspace linear solvers each of which is accelerated by a Schwarz preconditioner. The algorithm partitions and distributes the computational load evenly to a parallel computer. More details of the discretization of equations and the implemented algorithms can be found in our previous works [26], [27]. Fig. 5 shows a patient-specific arterial network partitioned into 8 subdomains each has a different color and each subdomain has a fairly equal number of elements to ensure a good load balance in parallel computing.

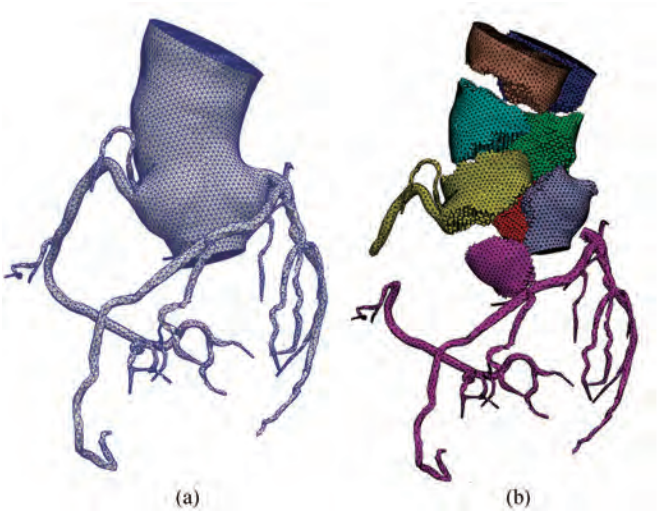

Fig. 5. Sketch view of computational mesh and domain partition. (a) The patient-specific computational domain was discreted by finite element method on a fully unstructured tetrahedral mesh. (b) The mesh was then partitioned into 8 subdomains (in different colors) and each subdomain has a fairly equal number of elements to ensure a good load balance in parallel computing.

The parallel solver is implemented using PETSc [28], and the computations are carried out on a computer with 10 computing nodes, each of which has two 12-core Intel Xeon E5-2692 v2 2.6 GHz CPU processors with 64 GB RAM. ParMETIS [29] is used for the mesh partition.

D. Clinical validation

To understand the impact to the hemodynamics of a catheter and a pressure wire, we first need to ensure that the simulation result with a pressure wire is consistent with the value obtained in the interventional measurement. In this study, the

main reference indicators used to calibrate the simulation are FFR and the time-averaged volume flow rate Q through the lesion subsegment. The clinical $\mathrm{FFR_{cli}}$ is measured by the pressure wire, according to the FFR clinical guidelines [30], the proximal pressure P_a is measured at the opening of the catheter. Therefore, in the numerical simulation, we also select this position as the proximal pressure monitoring point. The position for measuring the distal pressure P_d in the numerical simulation is referred to as the sensor position shown in the DSA images.

The time-averaged volume flow rate through the lesion subsegment Q is calculated by the thrombolysis in myocardial infarction frame count method [31] based on the DSA images. The method can be described as follows: we first calculate the volume of a certain blood vessel segment V_{seg} including the lesion based on the reconstructed three-dimensional geometric model. The start and the end point of the segment are as landmarks to see where the contrast agent arrives and usually located in a secondary branch, as shown in Fig. 6. Finally we obtain the time-averaged volume flow rate Q by V_{seg} and the time passing the segment. It should be noted that when calculating $Q_{\mathrm{num}}^{\mathrm{wire}}$, there is a certain amount of error if there are too few frames (high blood velocity) or uneven distribution of the contrast agent.

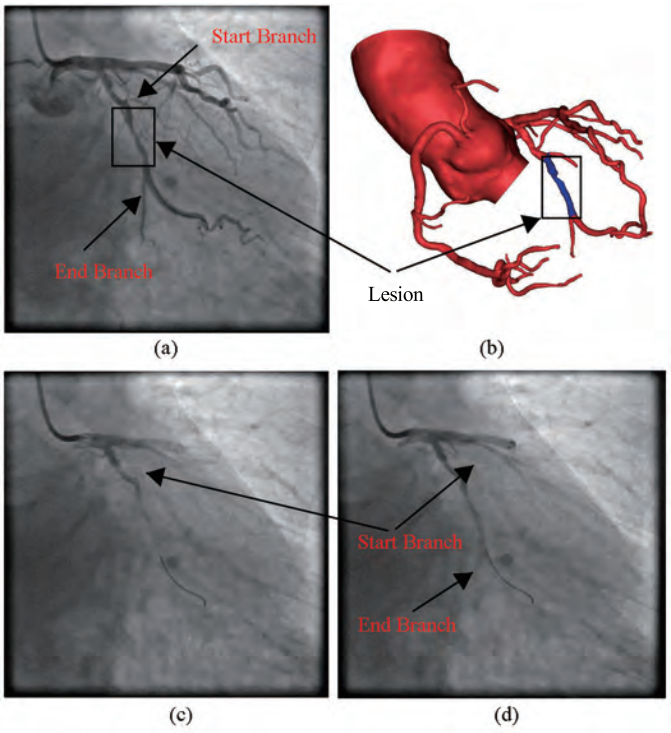

Fig. 6. Calculate time-averaged volume flow rate through the lesion subsegment. (a) Lesion subsegment in DSA image. (b) Lesion subsegment in the reconstructed 3D geometry of the artery. (c) and (d): Start frame and end frame corresponding to the start point and the end point of the lesion subsegment. We count the number of frames of blood flow through this segment, and finally obtain the time-averaged volume flow rate $\boldsymbol{Q}$ by the volume of lesion $\boldsymbol{V}_{\mathrm{seg}}$ and the number of frames per second passing through the segment.

With the fixed flow rate Q, we adjust the total resistance so that the computed values $\mathrm{FFR_{num}^{wire}}$ and $Q_{\mathrm{num}}^{\mathrm{wire}}$ with a catheter and a pressure wire match the clinically measured values $\mathrm{FFR_{cli}}$ and Q. The same boundary conditions are then applied to compute the flows without a catheter and a pressure wire to obtain the values of $\mathrm{FFR_{num}^{nowire}}$ and $Q_{\mathrm{num}}^{\mathrm{nowire}}$, as well as the detailed flow field. Base on the clinical measurements and computed values of six patients, we study the impact of the pressure wire, and discuss the results under different geometric characteristics, such as the size of the stenosis.

III. Results

The main results are summarized in Table II which includes three sets of values of FFR and Q for each patient: The stenosis ratio is measured in the three-dimensional geometry reconstructed from the CCTA images. The subjects have a coronary stenosis between 17.0% to 65.8%, the diameters of the narrowest region of the stenosis range from 1.06 mm to 2.94 mm, and the reference diameters range from 3.00 mm to 4.49 mm. The measured and computed flow rate Q through the lesion are also presented in this table. Due to the complexity of coronary blood flow, the average and maximum difference between $\mathrm{FFR_{num}^{wire}}$ and $\mathrm{FFR_{cli}}$ are around 2.2% and 6.6%, respectively.

TABLE II
THE MEASURED AND COMPUTED FRACTIONAL FLOW RESERVE AND TIME-AVERAGED VOLUME FLOW RATE THROUGH THE LESION.

Patient ID	RD (mm)	SD (mm)	Measurement	P_a (mmHg)	P_d (mmHg)	FFR	Q ($\mathrm{cm^3/s}$)
1	3.54	1.21	Invasive	71.0	40.0	0.563	
			CFD(with wire)	74.1	39.1	0.528	0.3981
			CFD(without wire)	74.4	47.2	0.634	0.4751
2	4.13	2.04	Invasive	74.0	65.0	0.878	
			CFD(with wire)	75.4	64.9	0.862	2.6556
			CFD(without wire)	74.8	67.7	0.906	2.7103
3	3.54	2.94	Invasive	76.0	71.0	0.934	
			CFD(with wire)	79.2	71.4	0.902	1.8375
			CFD(without wire)	78.3	72.8	0.930	1.8751
4	3.89	1.75	Invasive	74.0	66.0	0.892	
			CFD(with wire)	75.1	67.3	0.896	0.7594
			CFD(without wire)	75.3	69.6	0.924	0.7872
5	4.49	2.15	Invasive	74.0	67.0	0.905	
			CFD(with wire)	74.2	70.1	0.945	1.8365
			CFD(without wire)	73.4	70.2	0.956	1.8473
6	3.00	1.06	Invasive	67.0	56.0	0.840	
			CFD(with wire)	69.7	54.7	0.785	0.8323
			CFD(without wire)	69.6	58.0	0.833	0.8753

Notes: RD = reference diameter; SD = diameter of the narrowest region of the stenosis; P_a = proximal pressure; P_d = distal pressure; FFR = fractional flow reserve; Q = time-averaged volume flow rate through the lesion. For each patient, three sets of data are listed. "Invasive" represents the clinical invasive values (FFR is measured by pressure wire); "CFD(with wire)" and "CFD(without wire)" denote the computed results with and without the catheter and the pressure wire, respectively.

Some analysis of the results in Table II are provided in Table III. With the insertion of the catheter and the pressure wire, the changes of the proximal pressure P_a at the coronary entrance are not obvious, the differences $P_a{}^{\mathrm{wire}}$-$P_a{}^{\mathrm{nowire}}$ are -0.3 mmHg, 0.6 mmHg, 0.9 mmHg, -0.2 mmHg, 0.8 mmHg and 0.1 mmHg, respectively. Therefore, we conclude that the catheter has no significant impact on P_a or FFR. In contrast, the changes in the distal pressure P_d are obvious. Without exception, the catheter and the pressure wire reduces the value of P_d in all patients, the differences $P_d{}^{\mathrm{wire}}$-$P_d{}^{\mathrm{nowire}}$ are -8.1 mmHg, -2.8 mmHg, -1.4 mmHg, -2.3 mmHg, -0.1 mmHg and -3.3 mmHg, respectively. The maximum variation of P_d occurred in Patient 1 with -17.2%. It should be noted that,

all percentages are obtained from pressure drops at their corresponding hyperemic flow rates. Corresponding to P_a and P_d, the FFR of Patient 1 decreases from 0.634 to 0.528 (-16.8% decrease). For the other 5 patients, their FFRs decrease by -4.9%, -3.0%, -3.0%, -1.2% and -5.8%, respectively. The average FFR reduction for the six patients is 5.8%.

TABLE III

THE CHANGE OF FRACTIONAL FLOW RESERVE AND TIME-AVERAGED VOLUME FLOW RATE THROUGH THE LESION AFTER THE INSERTION OF CATHETER AND PRESSURE WIRE.

Patient ID	RWSA	ΔP_a (mmHg)	PP_a	ΔP_d (mmHg)	PP_d	ΔFFR	PFFR	ΔQ (cm^3/s)	PQ
1	8.6%	-0.3	-0.4%	-8.1	-17.2%	-0.107	-16.8%	-0.0770	-16.2%
2	3.0%	0.6	0.8%	-2.8	-4.1%	-0.044	-4.9%	-0.0547	-2.0%
3	1.5%	0.9	1.1%	-1.4	-1.9%	-0.028	-3.0%	-0.0376	-2.0%
4	4.1%	-0.2	-0.3%	-2.3	-3.3%	-0.028	-3.0%	-0.0278	-3.5%
5	2.7%	0.8	1.1%	-0.1	-0.1%	-0.012	-1.2%	-0.0108	-0.6%
6	11.3%	0.1	0.1%	-3.3	-5.7%	-0.049	-5.8%	-0.0430	-4.9%

Notes: RWSA = ratio of cross-sectional area of pressure wire to stenosis; P_a = proximal pressure; P_d = distal pressure; ΔP_a = change of P_a after the insertion of catheter and pressure wire; PP_a = percentage difference of P_a; ΔP_d = change of P_d after the insertion of catheter and pressure wire; PP_d = percentage difference of P_d; FFR = fractional flow reserve; ΔFFR = FFR change after the insertion of catheter and pressure wire; PFFR = percentage difference of FFR ; Q = time-averaged volume flow rate through the lesion; ΔQ = change of Q after the insertion of catheter and pressure wire; PQ = percentage difference of Q .

IV. Discussion

A. FFR and flow rate

Based on the results presented in Table III, we analyze the relationship between the changes of FFR and Q and the stenosis diameter and the stenosis ratio. The fitted curves are provided in Fig. 7.

The linear relationships between ΔFFR and SD (Fig. 7a) and between ΔQ and SD (Fig. 7d) illustrate that the smaller the absolute value of the stenosis diameter, the more the drop of FFR and Q. This means that the increase in the stenosis severity will increase the FFR and flow rate Q drop along the lesion. Fig. 7b and Fig. 7e indicate that the catheter and pressure wire cause more reduction of FFR and Q in lesions with greater stenosis ratio. Considering that in realistic lesions, the calculated stenosis ratio based on the diameter may not be able to accurately embody the complex shape of the coronary artery, in Fig. 7c and Fig. 7f, we also present the relationship between the ratio of the cross-sectional area of the pressure wire to the cross-sectional area of the stenosis and the variation of FFR and Q. Similar to the stenosis ratio, the trend that the larger RWSA, the more the FFR and Q decrease is also found in the curves ΔFFR-RWSA and ΔQ-RWSA.

The results presented in Tab. III and Fig. 7 show clearly that the presence of a catheter and pressure wire in the coronary artery adds extra volume and resistance to blood flow, and therefore lead to the increase of the pressure drop and the decrease of the volume of the flow through the lesion, and as a result, there is a decrease of the FFR. The impact of the decreased FFR on the outcome of the diagnosis varies across the spectrum of stenosis. Specifically, for the physiologically mild lesions, in which invasive FFR procedures rarely performed, the superposition of a large measured FFR ($\geq$ 0.90) and a small ΔFFR will not change the diagnosis, for example, Patient 3. For the intermediate lesions, such as the other 5 patients, the correction may change the outcome of the diagnosis. Take Patient 6 as an example, the removal of the catheter and the pressure wire changes FFR from 0.785 (54.7/69.7) to 0.833 (58.0/69.6). Thus, different diagnoses are obtained if the decision is made based on the critical value of FFR which is 0.8. Although no cases with severe stenosis were included in this work, considering that the pressure wire may exaggerate the stenosis and cause a decrease in the measured FFR, and the smaller the stenosis diameter, the larger the ΔFFR becomes (Fig. 7a and Fig. 7c), we still recommend correcting the computed FFR for the severe stenosis. Consequently, the relationship between FFR_{num}^{nowire} and FFR_{cli} needs to be carefully considered, so as not to underestimate the degree of ischemia and lead to misdiagnosis of lesion severity. With this regard, the curves shown in Fig. 7 can be helpful in interpreting the FFR results.

In view of the fact that the FFR value (0.8 is the watershed) measured by the interventional catheter and pressure guide wire is the gold standard for clinical diagnosis, the current rapidly developing noninvasive diagnostic technology such as CFD usually does not consider the influence of catheters and guide wires. As far as we know, in noninvasive FFR technology, there are many different types of blood flow models and empirical parameters. The impact of the pressure wire may be reduced by adjusting the empirical parameters. However, there are various stenosis subgroups, as well as other complex lesions, such as bifurcation, tandem lesions and multi-vessel lesions, a more clear inspection of the insertion of the pressure wire on FFR needs to be investigated. Further more, our blood flow model and boundary conditions still need to be improved to obtain more accurate FFR values, for example, considering the interaction between the myocardium and coronary vessels under the pulsating condition. Nevertheless, we believe the noninvasive FFR should have its own cutoff value instead of using the one chosen for the invasive FFR.

B. Flow pattern

In addition to the changes of the FFR and Q values, the dynamics of the blood flow is also changed. In this section, we choose Patient 6 as an example to show the details of flow changes through the coronary arteries and the stenosis with and without the presence of the catheter and pressure wire. We show the time-averaged pressure and transient velocity profiles across three different cross-sectional regions including: (A) inlet of coronary, location of the proximal pressure sensor, (B) stenosis and (C) location of the distal pressure sensor, as illustrated in Figs. 8-11.

The time-averaged pressure profiles are presented in Fig. 8 and Fig. 9. Comparing with the results without the catheter and pressure wire, it is clear that there is a negligible change at location A and an obvious decrease at both locations B and C. Note that the presence of the catheter and pressure wire has little effect on the pressure distribution at locations A and C, which are the locations of proximal and distal pressure sensors respectively. But at location B where the stenosis locates, the range of the pressure changes

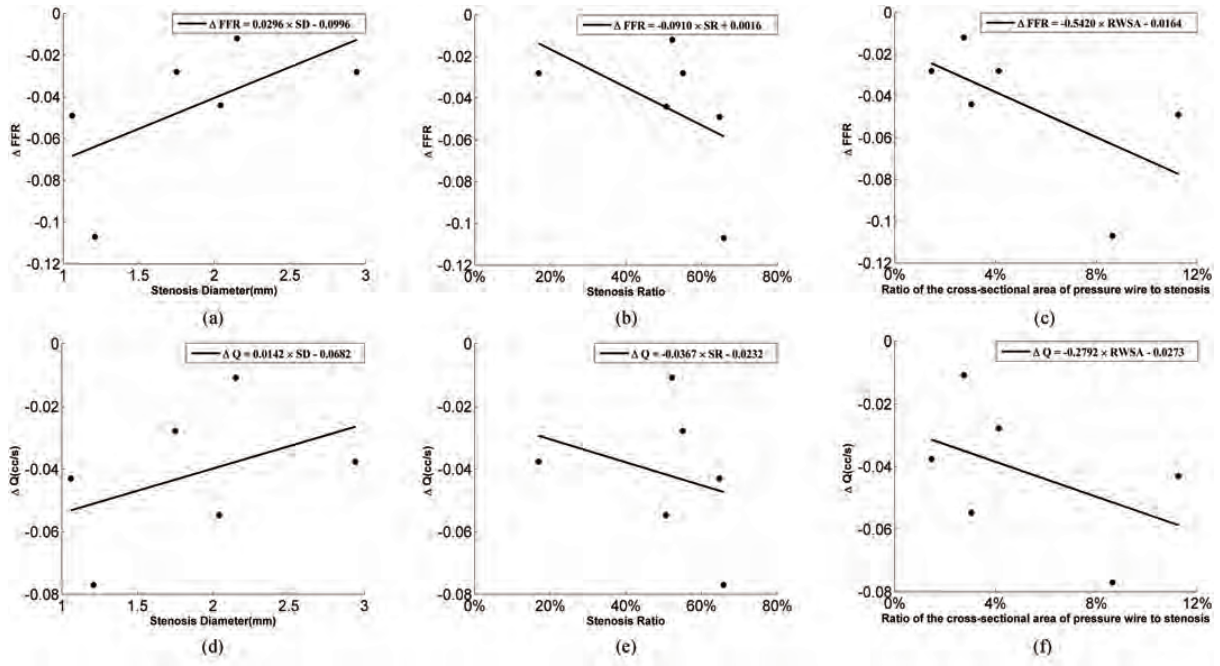

Fig. 7. Linear correlations of the reduction of fractional flow reserve and the flow rate with the stenosis parameters. FFR = fractional flow reserve; ΔFFR = FFR change after the insertion of catheter and pressure wire; $\boldsymbol{Q}$ = time-averaged volume flow rate through the lesion; $\Delta\boldsymbol{Q}$ = change of $\boldsymbol{Q}$ after the insertion of catheter and pressure wire; SD = fitting diameter of the narrowest region of the stenosis; SR = stenosis ratio; RWSA = ratio of cross-sectional area of pressure wire to stenosis. After the insertion of the catheter and the pressure wire, the relationship between: (a) SD and ΔFFR: (ΔFFR=0.0296$\times$SD-0.0996). (b) SR and ΔFFR: (ΔFFR=0.0910$\times$SR+0.016). (c) RWSA and ΔFFR: (ΔFFR=-0.5420$\times$RWSA-0.0164). (d) SD and $\Delta\boldsymbol{Q}$: ($\Delta\boldsymbol{Q}$=0.0142$\times$SD-0.0682). (e) SR and $\Delta\boldsymbol{Q}$: ($\Delta\boldsymbol{Q}$=-0.0367$\times$SR-0.0232). (f) RWSA and $\Delta\boldsymbol{Q}$: ($\Delta\boldsymbol{Q}$=-0.2792$\times$RWSA-0.0273).

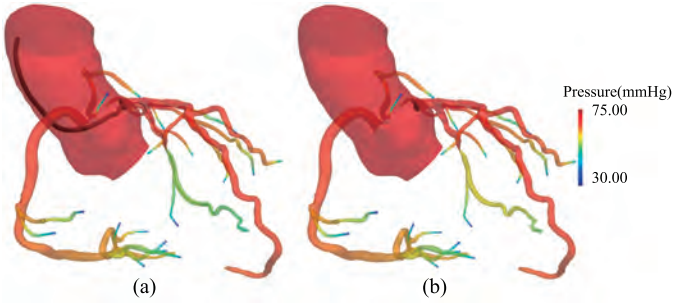

Fig. 8. Global view of the comparison of the time-averaged pressure profiles. (a) With catheter and pressure wire. (b) Without catheter and pressure wire. The presence of the pressure wire increases the pressure drop downstream of the left anterior descending stenosis.

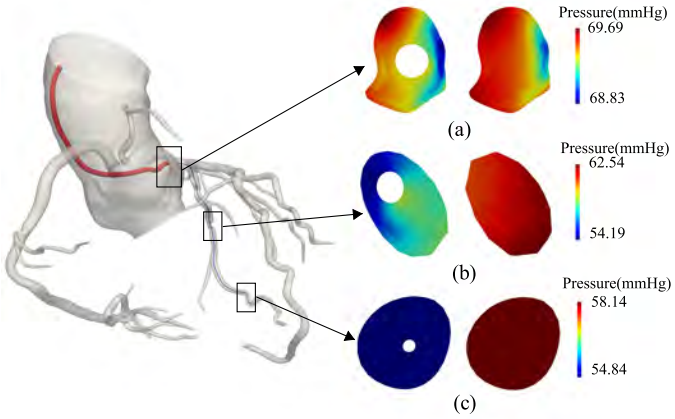

Fig. 9. Comparison of the time-averaged pressure profiles with and without catheter and pressure wire. (a) At cross-section A: the junction of the catheter and the pressure wire. (b) At cross-section B: at the stenosis. (c) At cross-section C: at the $\boldsymbol{P_d}$ measurement point.

goes from 1.79 mmHg (min:60.75 mmHg ; max:62.54 mmHg) to 4.72 mmHg (min:54.19 mmHg; max:58.91 mmHg). This means that even if the pressure sensor is placed at location B, the measured pressure value and the corresponding FFR may vary by more than 8.7% and 9.7%, respectively. In other words, if the distal sensor is too close to the lesion, it may cause the pressure value to fluctuate even if it is placed at the same section but different direction. This also explains from another perspective that the distal measurement position of the pressure sensor needs to be placed in the normal blood vessel distal to the lesion, for example, 3.0 cm downstream of the lesion.

The transient axial velocity profiles corresponding to the systolic peak and the end of diastole are shown in Fig. 10, and Fig. 11, respectively. The velocity figures show that: (1) whether it is in systole or diastole, the existence of the catheter and the pressure wire changes not only the velocity magnitude' range, but also the distribution, especially near the stenosis (location B) and distal to the stenosis (location C); (2) Even though the results in Table III show that the presence of the catheter and the pressure wire reduces the flow through the lesion, which implies that the average flow velocity decreases, at the same time, as shown at locations A and B, the velocity range is wider, i.e., the maximum velocity is higher and the distribution is more even. This is because the presence of the catheter and the pressure wire reduces the cross-sectional

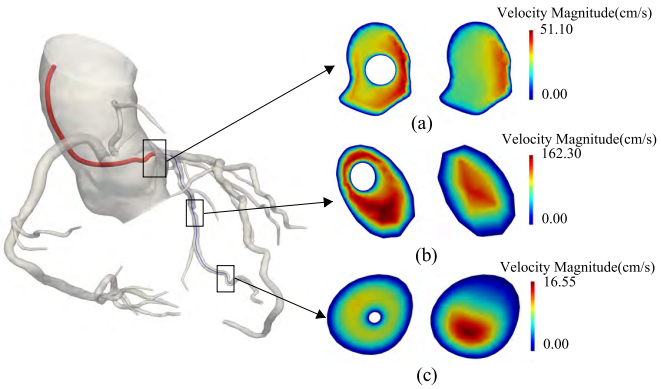

Fig. 10. Comparison of the velocity profiles at the end of diastole with and without catheter and pressure wire. (a) At cross-section A: the junction of the catheter and the pressure wire. (b) At cross-section B: at the stenosis. (c) At cross-section C: at the P_d measurement point.

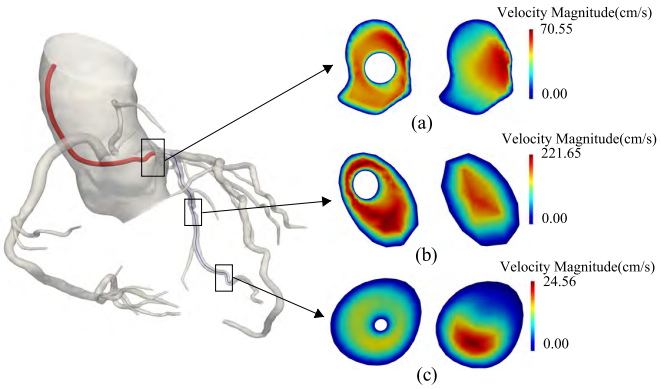

Fig. 11. Comparison of the velocity profiles at the systolic peak with and without catheter and pressure wire. (a) At cross-section A: the junction of the catheter and the pressure wire. (b) At cross-section B: at the stenosis. (c) At cross-section C: at the P_d measurement point.

area of the blood vessel, and the local flow velocity therefore needs to be increased to compensate for the downstream blood supply; (3) Different from locations A and B, the pressure wire reduces the maximum velocity at location C, where a secondary branch (Branch 1) downstream of the lesion starts, this implies that the reduced flow through this branch offsets the effect of the reduced section area. Beside reducing the total time-averaged volume flow rate thought the lesion from $0.8753\,\mathrm{cm}^3/\mathrm{s}$ to $0.8323\,\mathrm{cm}^3/\mathrm{s}$, the insertion of the pressure wire can also redistribute the blood flows in the downstream branches.

The 3D velocity streamlines at the systole stage are shown in Fig. 12, which shows a small disturbance of the flow in the coronary artery. A comparison of the global streamlines indicates that the presence of the catheter and the pressure wire not only increases the magnitude of the velocity in the lesion where the pressure wire is inserted, but also affects the velocity in other coronary arteries such as the branches of the right coronary artery, even if no pressure wire is inserted into them. Near the left posterior aortic sinus, where the left coronary artery starts, the catheter causes a small perturbation; i.e., the structure and the size of the vortex in this area are changed. Near the lesion, the pressure wire only has some noticeable effect in the downstream area adjacent to the lesion, with changes in the size of the vortex and the velocity. The flow pattern is not observably altered in the upstream area and the downstream area away from the lesion.

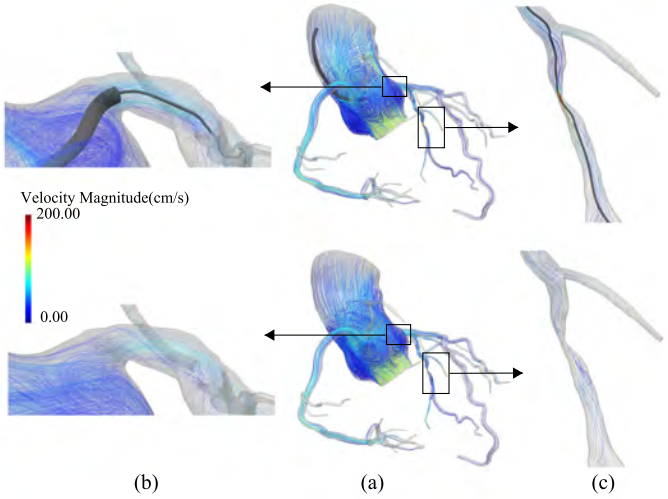

Fig. 12. Comparison of 3D streamlines at the systolic peak stage with and without catheter and pressure wire. (a) Global view. (b) At the junction of the catheter and the pressure wire. (c) At the stenosis.

V. Conclusion

In the past few years, noninvasive FFR technology has shown to have tremendous potential to evaluate the functional significance of coronal stenosis. Considering the fact that the existence of the pressure wire in the artery aggravates the obstructive effect of the lesion and therefore causes the measured FFR to be less than the actual value, we studied the impact of the pressure wire on the FFR and the hemodynamics of the coronary arteries. This study clarified that placing a pressure wire through a catheter in the coronary arteries to measure FFR can cause a pressure drop distal to the stenosis and consequently results in a reduction in FFR, which is proportional to the minimum diameter of the stenosis. Moreover, the placement of the pressure wire will decrease the flow rate passing the stenosis, which is proportional to the minimum diameter of the stenosis. According to these findings, we conclude that the placement of a pressure wire through a cardiac catheter can cause an adverse impact on FFR. Considering the fact that the catheter and the pressure wire model are excluded in all existing CFD-based noninvasive FFR technologies, the computed FFR requires a correction according to the characteristics of the lesion or a different cut-off value should be used instead of the one chosen for the invasive FFR.

References

[1] F.-J. Neumann et al., "2018 ESC/EACTS Guidelines on myocardial revascularization", *Eur. Heart J.*, vol. 40, no. 2, pp. 87–165, 2018.

[2] J. Adjedj et al., "Comparison of coronary angiography and intracoronary imaging with fractional flow reserve for coronary artery disease evaluation: An anatomical-functional mismatch", *Anatol. J. Cardiol.*, vol. 20, no. 3, pp. 182–189, 2018.

[3] P. A. Tonino et al., "Fractional flow reserve versus angiography for guiding percutaneous coronary intervention", *N. Engl. J. Med.*, vol. 360, no. 3, pp. 213–224, 2009.
[4] S. A. Chamuleau et al., "Usefulness of fractional flow reserve for risk stratification of patients with multivessel coronary artery disease and an intermediate stenosis", *Am. J. Cardiol.*, vol. 89, no. 4, pp. 377–380, 2002.
[5] R. C. Mathew, et al., "Computed tomography fractional flow reserve to guide coronary angiography and intervention", *Interv. Cardiol. Clin.*, vol. 7, no. 3, pp. 345–354, 2018.
[6] N. H. Pijls et al., "Measurement of fractional flow reserve to assess the functional severity of coronary-artery stenoses", *N. Engl. J. Med.*, vol. 334, no. 26, pp. 1703–1708, 1996.
[7] S. Benenati, et al., "Invasive in the cath-lab assessment of myocardial ischemia in patients with coronary artery disease: When does the gold standard not apply", *Cardiovasc. Revasc. Med.*, vol. 19, no. 3, Part B, pp. 362–372, 2018.
[8] K. D. Ashtekar et al., "In vitro quantification of guidewire flow-obstruction effect in model coronary stenoses for interventional diagnostic procedure", *J. Med. Dev.*, vol. 1, no. 3, pp. 185–196, 2007.
[9] R. K. Banerjee et al., "Influence of newly designed monorail pressure sensor catheter on coronary diagnostic parameters: An in vitro study", *J. Biomech.*, vol. 47, no. 3, pp. 617–624, 2014.
[10] S. Tadaoka et al., "Accuracy of 20-mhz doppler catheter coronary artery velocimetry for measurement of coronary blood flow velocity", *Cathet. Cardiovasc. Diagn.*, vol. 19, no. 3, pp. 205–213, 1990.
[11] R. Torii et al., "A computational study on the influence of catheter-delivered intravascular probes on blood flow in a coronary artery model", *J. Biomech.*, vol. 40, no. 11, pp. 2501–2509, 2007.
[12] E. Rajabi-Jaghargh et al., "Effect of guidewire on contribution of loss due to momentum change and viscous loss to the translesional pressure drop across coronary artery stenosis: an analytical approach", *Biomed. Eng. Online*, vol. 10, no. 1, pp. 1–22, 2011.
[13] A. S. Roy et al., "Delineating the guide-wire flow obstruction effect in assessment of fractional flow reserve and coronary flow reserve measurements", *Am. J. Physiol. Heart Circ. Physiol.*, vol. 289, no. 1, pp. H392–H397, 2005.
[14] C. A. Taylor et al., "Computational fluid dynamics applied to cardiac computed tomography for noninvasive quantification of fractional flow reserve", *J. Am. Coll. Cardiol.*, vol. 61, no. 22, pp. 2233–2241, 2013.
[15] B. L. Nørgaard et al., "Diagnostic performance of noninvasive fractional flow reserve derived from coronary computed tomography angiography in suspected coronary artery disease: the NXT trial (analysis of coronary blood flow using CT angiography: Next steps)", *J. Am. Coll. Cardiol.*, vol. 63, no. 12, pp. 1145–1155, 2014.
[16] P. S. Douglas et al., "Clinical outcomes of fractional flow reserve by computed tomographic angiography-guided diagnostic strategies vs. usual care in patients with suspected coronary artery disease: the prospective longitudinal trial of FFR_{CT}: outcome and resource impacts study", *Eur. Heart J.*, vol. 36, no. 47, pp. 3359–3367, 2015.
[17] J. M. Carson et al., "Non-invasive coronary CT angiographyderived fractional flow reserve: A benchmark study comparing the diagnostic performance of four different computational methodologies", *Int. J. Numer. Meth. Bio.*, vol. 35, no. 10, pp. e3235–e3256, 2019.
[18] C. M. Cook et al., "Diagnostic accuracy of computed tomography-derived fractional flow reserve: a systematic review", *JAMA Cardiology*, vol. 2, no. 7, pp. 803–810, 2017.
[19] J. W. Hirshfeld and A. S. Nathan, "QFR and FFR_{CT}: Accurate enough", *J. Am. Coll. Cardiol. Intv.*, vol. 12, no. 20, pp. 2060–2063, 2019.
[20] M. Moscucci, Grossman & Baim's Cardiac Catheterization, Angiography, and Intervention, 9th ed. Philadelphia, PA, USA:Lippincott Williams & Wilkins, 2020.
[21] P. Segers et al., "Systemic and pulmonary hemodynamics assessed with a lumped-parameter heart-arterial interaction model", *J. Eng. Math.*, vol. 47, no. 3, pp. 185–199, 2003.
[22] I. E. Vignon-Clementel et al., "Outflow boundary conditions for 3D simulations of non-periodic blood flow and pressure fields in deformable arteries", *Comput. Method Biomec.*, vol. 13, no. 5, pp. 625–640, 2010.
[23] F. Kong et al., "An efficient parallel simulation of unsteady blood flows in patient-specific pulmonary artery", *Int. J. Numer. Method Biomed. Eng.*, vol. 34, no. 4, p. e2952, 2018.
[24] L. Luo et al., "A nonlinear elimination preconditioned inexact Newton method for blood flow problems in human artery with stenosis", *J. Comput. Phys.*, vol. 399, p. 108926, 2019.
[25] R. Chen et al., "A parallel non-nested two-level domain decomposition method for simulating blood flows in cerebral artery of stroke patient", *Int. J. Numer. Method Biomed. Eng.*, vol. 36, no. 11, p. e3392, 2020.
[26] Z. Yan et al., "Numerical aerodynamic simulation of transient flows around car based on parallel NewtonKrylovSchwarz algorithm", *Appl. Anal.*, vol. 100, no. 7, pp. 1501–1513, 2021.
[27] Z. Yan et al., "Large eddy simulation of the wind flow in a realistic full-scale urban community with a scalable parallel algorithm", *Comput. Phys. Commun.*, vol. 270, p. 108170, 2022.
[28] S. Balay et al., "PETSc Users Manual", Argonne National Laboratory, IL, Tech. Rep. ANL-95/11 - Revision 3.14, 2021.
[29] G. Karypis and V. Kumar, "ParMETIS–parallel graph partitioning and fill-reducing matrix ordering, Version 4", University of Minnesota, Minneapolis, MN, 2014.
[30] G. N. Levine et al., "2011 ACCF/AHA/SCAI guideline for percutaneous coronary intervention", *J. Am. Coll. Cardiol.*, vol. 58, no. 24, pp. e44–e122, 2011.
[31] C. M. Gibson et al., "TIMI frame count", *Circulation*, vol. 93, no. 5, pp. 879–888, 1996.